Journal of Molecular Structure 1240 (2021) 130504

Contents lists available at ScienceDirect

Journal of Molecular Structure

journal homepage: www.elsevier.com/locate/molstr

Crystal structure, mosquito larvicidal & antifungal activity of 3–*tert*–butyl–7-(2,3,4-trimethoxyphenyl)-4*H*-[1,3,4]thiadiazolo[2,3-*c*][1,2,4]triazin-4-one

Chandraprabha V. J[a], Jagadeesh Prasad Dasappa[a,*], Gayathri B. H[a], Madan Kumar S[b], B. Shivarama Holla[c], Ravindra R. Kamble[d], Prashantha Naik[e]

[a] Dept. of Chemistry, Mangalore University, Mangalore, Karnataka State, 574199, India
[b] IOE, Vijnana Bhavan, University of Mysore, Mysore, Karnataka State, 570006, India
[c] Dept of Chemistry, S.D.M. Autonomous College, Ujire, Mangalore, Karnataka State, 574240, India
[d] Dept of Chemistry, Karnatak University, Dharwad, Karnataka State, 580003, India
[e] Dept. of Biosciences, Mangalore University, Mangalore, Karnataka State, 574199, India

ARTICLE INFO

Article history:
Received 12 January 2019
Revised 10 April 2021
Accepted 12 April 2021
Available online 1 May 2021

Keywords:
Triazinone
Crystal structure
Hirshfeld surfaces
Thermal analysis
Larvicidal activity

ABSTRACT

The title compound 3–tert–butyl–7-(2,3,4-trimethoxyphenyl)-4*H*-[1,3,4]thiadiazolo[2,3-*c*][1,2,4]triazin-4-one was prepared and characterized using single crystal X-ray diffraction, thermal & Uv-Vis analysis, FTIR, NMR (^{1}H, ^{13}C) and Mass spectral studies. The intercontacts in the crystal structure were analyzed and quantified using Hirshfeld surfaces computational method. Intermolecular hydrogen bonds C12—H12A…O4, C13—H13C…O4, C15—H15A…O2 and C16—H16B…O3 connects the molecule in the crystal structure. The intramolecular hydrogen bond of the type C—H …N was observed. Intercontacts H…H, O…H and N…H shows more contributions towards Hirshfeld surfaces. Thermal analysis indicates the title compound starts to degrade at 216.9 °C. In addition, mosquito larvicidal activity and antifungal activity were performed.

Introduction

The demands of the global market and advancements in the current science and technology have augmented the research in the field of the drug synthesis. The novel inventions and available literature on triazinone derivatives have drawn considerable interest because, the compound bearing triazinone moiety are of enormous importance in the field of medicine. They possess attractive biological activities such as, antimicrobial [1], antioxidant [2], antibacterial [3], antitubercular [4], antitumour and antimetastatic activities [5]. In addition to these, triazinone derivatives have also shown applications as herbicide residues [6], antifish parasites [7] and mosquito-larvicidal activity [8]. Based on the pharmacological importance of triazinone derivatives, following reaction scheme was taken up & synthesized the title compound.

2. Experimental details

2.1. Materials and physical measurements

The starting materials trimethyl pyruvic acid (grade AR), thiocarbohydrazide (grade AR) and 2,3,4-trimethoxy benzoic acid were procured from Sigma Aldrich (India), Alfaaesar (U. K.) and were used as such. The melting points of the target compound 3–*tert*–butyl–7-(2,3,4-trimethoxyphenyl)–4*H*-[1,3,4]thiadiazolo[2,3-*c*][1,2,4]triazin-4-one was determined by open capillary method and was uncorrected. The completion of the reaction was monitored by TLC on Merck silica gel 60 F_{254} coated alumina plates. The IR spectrum (cm^{-1}) was recorded on a Shimadzu-FTIR 577 infrared spectrometer by KBr pellets. The ^{1}H NMR and ^{13}C NMR spectra was recorded on Brucker AMX-400(400 MHz) spectrometer using $CDCl_3$ as solvent and TMS as the internal standard. The mass spectrum was recorded on Perkin-Elmer 018444Y, triple quadrapole LC-MS spectrometer. The elemental analysis (C, H, N and S) was carried out on Elementar Vario EL III analyzer.

* Corresponding author.
E-mail address: jprasad2003@gmail.com (J.P. Dasappa).

https://doi.org/10.1016/j.molstruc.2021.130504
0022-2860/

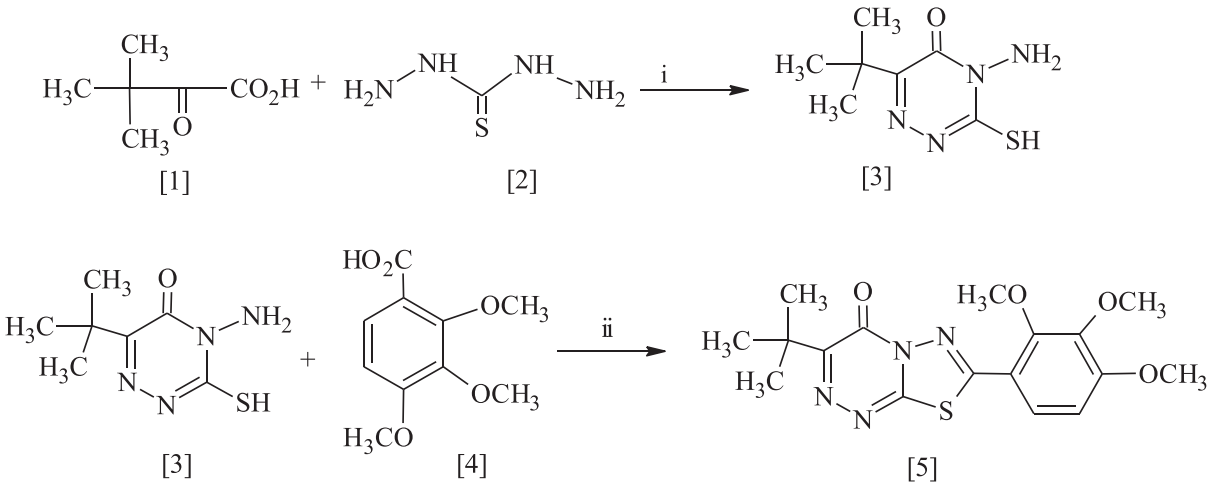

Scheme 1. Reaction conditions: i) Ethanol, 60 °C, refluxed for 12 h, ii) $POCl_3$, 90 °C, refluxed for 8 h.

2.2. Material synthesis

The compound (5) was synthesized according to the detailed procedure from the literature [4,8]. The equimolar mixture of 3,3-dimethyl-2-oxobutanoic acid (trimethyl pyruvic acid, 0.01 mol) (1) and thiocarbohydrazide (0.01 mol) (2) were refluxed in ethanol solvent for 12 h to get a highly pure reaction intermediate 4-amino-6–*tert*–butyl–3-sulfanyl-1,2,4-triazin-5(4*H*)-one (3) which was later condensed with equimolar ratio of 2,3,4-trimethoxy benzoic acid (0.01 mol) (4) in the presence of $POCl_3$ at 90 °C for 8 h under dry condition. The reaction mixture was cooled and poured into crushed ice, drop wise with vigorous shaking. The solid product separated was later filtered using filter paper and recrystallized from ethanol to get target compound. Melting point of the compound was observed as 140–146 °C (5) (Scheme 1).

2.3. Growth of single crystal 3–tert–butyl–7-(2,3,4-trimethoxyphenyl)–4H-[1,3,4]thiadiazolo[2,3-c][1,2,4]triazin-4-one

The compound (5) was dissolved in ethanol and heated to a high temperature and then filtered using Whatman No 41 filter paper to remove suspended impurities and kept aside without any mechanical disturbance for growth of crystals by slow evaporation at room temperature. After about a week transparent and colorless single crystal of the dimensions of 0.23 × 0.24 × 0.31 mm was obtained by slow evaporation technique. The grown crystals were repeatedly recrystallized in ethanol to get good quality crystals. The crystal had good compositional stability and showed no degradation when kept in the open air for several months.

2.4. Spectroscopic characterization of the title compound

IR Spectrum of the crystal compound showed the aliphatic C–H stretching band at 2955 cm^{-1} and aromatic C–H stretching band at 3078 cm^{-1}. The absorption appeared at 1700 cm^{-1} is due to carbonyl stretching frequency. The bands observed at 1591, 1514, 1491 & 1452 cm^{-1} are due to $C = N$ and $C = C$ groups.

In ^1H NMR the compound showed a sharp singlet at δ 1.91 ppm corresponding to nine methyl protons of tertiary butyl group. The three methoxyl groups have appeared as three singlets at δ 4.11, 3.97 and 3.91 ppm respectively.

The LC Mass of the compound showed a base peak at *m/z* 377, molecular ion peak at *m/z* at 378 and $m + 1$ peak at *m/z* 389. These analyses confirmed the formation of compound.

2.5. X-ray data collection, structure determination and refinement

The X-ray analysis of the molecule (5) was carried out at a temperature of 296 K on a Rigaku Saturn 724 diffractometer using graphite monochromated Mo-Kα radiation. A complete set of data was processed using *CrystalClear* [9]. The single crystal was solved by direct methods and refined by full-matrix least squares method on F^2 using *SHELXS* and *SHELXL* programs [10], the crystallographic study revealed that the crystal had dimensions of 0.23 × 0.24 × 0.31 mm^3 with absorption coefficient 0.210 mm^{-1}. The non-hydrogen atoms present in the molecule were identified in the first Fourier map itself and subjected to Full-matrix least squares refinement using SHELXL programs. The thermal ellipsoid plot at 50% probability of the compound (5) is represented in Fig. 1. The ORTEP and molecular packing diagrams were plotted using MERCURY [11]. A summary of experimental and crystallographic data for the compound (5) is given in Table 1. Packing of the compound (5) viewed along different axis is represented in Fig. 2. The details of crystallographic information have been deposited at the CCDC NO. 1,541,667, which includes supplementary crystallographic data and can be obtained free of charge at www.ccdc.cam.ac.uk/conts/retrieving.html [or from the Cambridge Crystallographic Data center (CCDC), 12 Union Road, Cambridge CB2 1EZ, UK; fax: +44(0)1223 762,911; email: deposit@ccdc.cam.ac.uk]

3.4. UV–visible spectral analysis

The UV–Vis spectrum [12] was recorded in the range up to 800 nm using CARY 5E UV–VIS-NIR Spectrophotometer and the spectrum is shown in Fig. 3. The presence of groups like $C = C$, $C = N$, $C = O$, due to delocalization of electrons and increased conjugation, the absorbance is shifted to the higher wavelength. The maximum λ_{max} for the compound (5) was observed at 350 nm which is in UV region, indicating that the molecule is highly active and show maximum absorbance in UV region. Hence the molecule is colorless.

3.5. Elemental analysis

The elemental analysis of the crystal showed coincidence between the experimental and calculated percentage values which confirms the formation of the compound (5) in the stoichometric ratio.

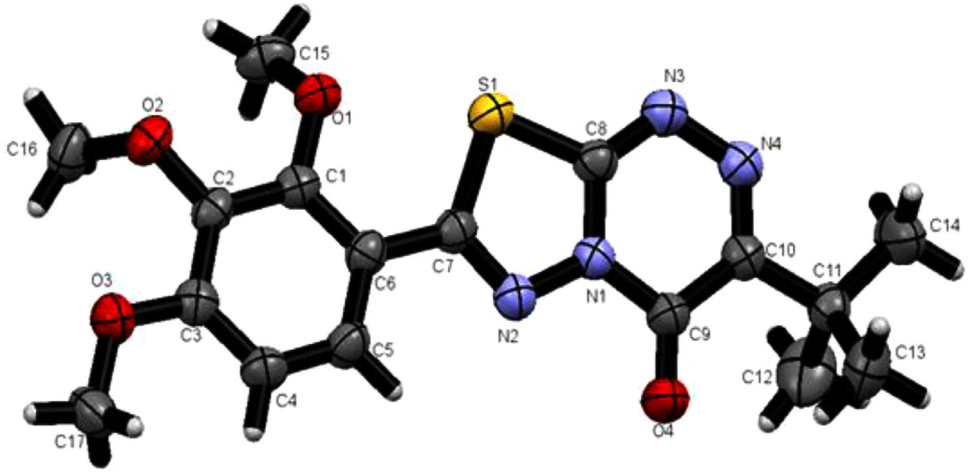

Fig. 1. ORTEP diagram of the compound (5). Displacement ellipsoids are drawn at the 50% probability.

Table 1
Crystal data and structure refinement for compound (5).

Empirical formula	: $C_{17}H_{20}N_4O_4S$
Formula weight	: 376.43
Temperature	: 293(2) K
Wavelength	: 0.71075 Å
Crystal system space group	: Orthorhombic,: *Pbca*
Unit cell dimensions	: a = 13.1873(6) Å: b = 8.7671(4) Å: c = 31.2626(10) Å: $\alpha = \beta = \gamma = 90$ °
Volume	: 3614.4(3) Å^3
Z Calculated density	: 8: 1.383 Mg/m^3
Absorption coefficient	: 0.210 mm^{-1}
$F_{(000)}$	: 1584
Crystal size	: 0.23 × 0.24 × 0.31 mm
Theta range for data collection	: 2.0 to 31.1°
Limiting indices	: $-18 \leq h \leq 17$, $-12 \leq k \leq 12$, $-45 \leq l \leq 44$
Reflections collected / unique[R(int)]	: 47,009/5561 [0.050]
Refinement method	: Full-matrix least-squares on F^2
Data / restraints / parameters	: 4136 / 0 / 241
R value	: 0.0496
Goodness-of-fit on F^2	: 1.05
Largest diff. peak and hole	: 0.26 and −0.26 e. Å^{-3}
CCDC number	: 1,541,667

Elements	Observed mass percentage	Calculated mass percentage
C	54.18	54.24
H	5.28	5.36
N	14.00	14.18
S	8.89	8.92

3.6. Thermogravimateric analysis

The stability of the compound (5) was determined by thermo gravimetric analysis [12], over the temperature range of 50 °C-500 °C under nitrogen atmosphere and the corresponding thermogram is presented in Fig. 4-6. The thermogram represented two derivative curves (Figs. 4 and 5), the major weight loss was at 260.65 °C before the start of the decomposition and another at 310.8 °C. The phase transition of the compound was not observed until the material melts. The absence of weight loss around 100 °C indicated that there was no water of crystallization in the molecular structure. A sharp endothermic dip in DSC at 216.9 °C indicated the melting point of the material. The sharpness of this endothermic peak showed good degree of crystallinity and purity of the material, which was further confirmed by melting point apparatus. When the compound was further heated above 216.9 °C it decomposed and resulted in the formation of volatile substances, probably carbon dioxide and CO molecule. The next stage of decomposition was at 260.65 °C corresponds to the decomposition of residues. The transition from amorphous to crystalline solid was an exothermic process, and resulted in a sharp peak in DSC signal. As the temperature increased the sample eventually reached its melting point. Thus, from thermal analyses, it was seen that the crystal could be utilized for device applications in the field of optoelectronics and photonics up to 216.9 °C.

3.7. X-ray diffraction studies

The single crystal X-ray diffraction studies of the compound (5, Fig. 1) revealed that it crystallizes in orthorhombic system [space group of *Pbca*]. The number of atoms per unit cell, $Z = 2$, with the lattice parameters a = 13.1873(6) Å, b = 8.7671(4) Å, c = 31.2626(10) Å with bond angles $\alpha = \beta = \gamma = 90°$ and volume 3614.4(3) Å^3. The crystal structure (Fig. 2, Table 2) is stabilized with intermolecular hydrogen bonds C12—H12A…O4, C13—H13C…O4, C15—H15A…O2 and C16—H16B…O3. In addition, weak short contacts, Cg1:S1/C7/N2/N1/C8…Cg3:C1C6 (distance 3.8593 (8)Å) and Cg2:N1/C8/N3/N4/C10/C9…

Cg3 (distance 3.7948(9) Å).

3.8. Hirshfeld surface analysis

The compound under investigation was analyzed for molecular three dimensional Hirshfeld surfaces and two-dimensional fingerprint plots shows that the intermolecular H…H (47.0%), H…O

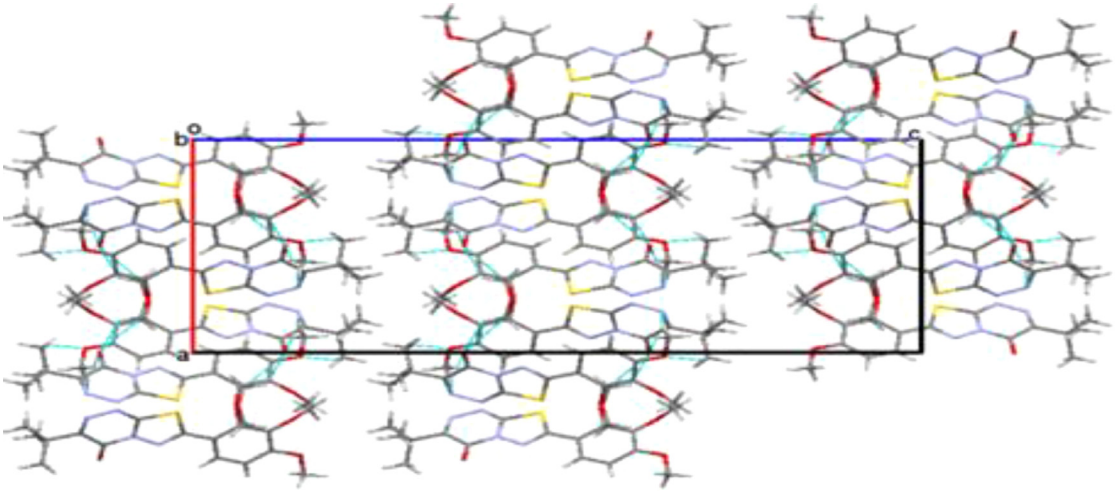

Fig. 2. Packing of the compound (5): view along (b) axis. Dotted lines represent weak contacts.

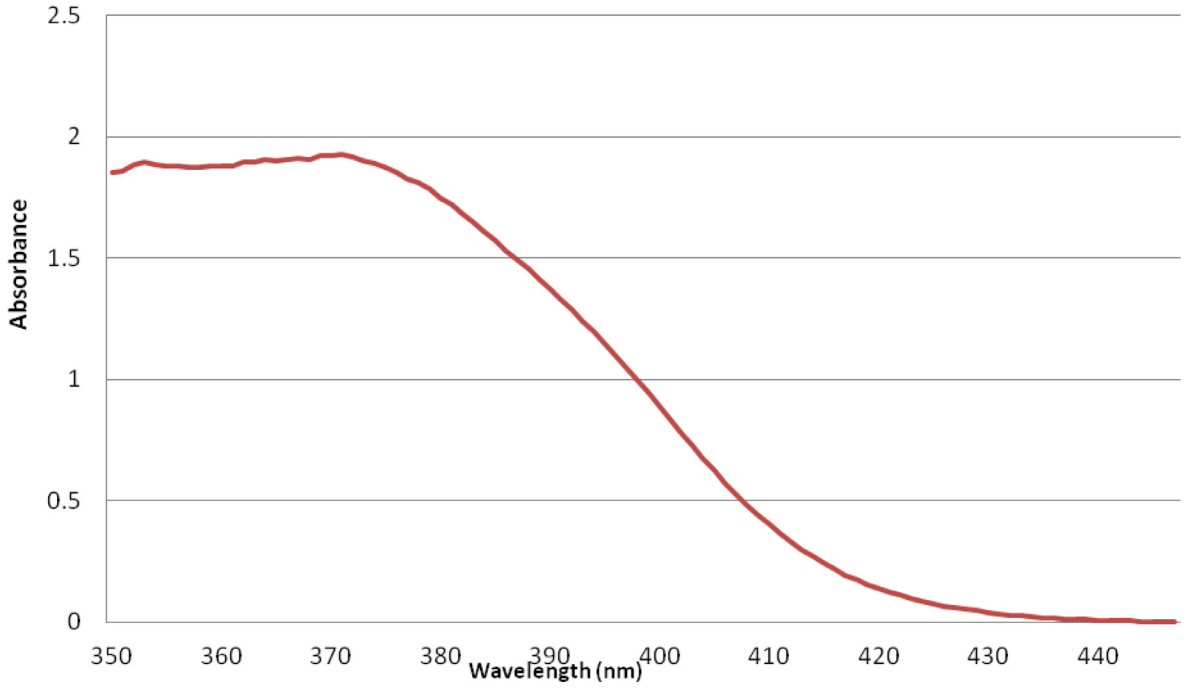

Fig. 3. UV-visible spectrum.

Table 2
Intramolecular Hydrogen-bonding interactions and geometry (Å^0).

D—H…A	D-H	H…A	D….A	D—H…A
C5—H5…N2	0.93	2.50	2.810(2)	100
C12—H12A…O4	0.96	2.48	3.083(3)	121
C13—H13C…O4	0.96	2.39	3.042(3)	124
C15—H15A…O2	0.96	2.51	2.922(2)	106
C16—H16B…O3	0.96	2.34	2.932(2)	118

(16.8%), N…H (12.2%), C…H (6.8%) has major contributions in the crystal packing. The partitioning of space with Hirshfeld surfaces enables the analysis of fingerprint molecular interactions in crystalline environments. The crystallographic information file (cif) was imported to the Crystal Explorer to generate the Hirshfeld surfaces. The Hirshfeld surface of the crystal is as shown in Fig. 7. The intermolecular contacts present in the crystal structures are quantified and visualized using Hirshfeld surfaces computational method [13–15]. Hirshfeld surfaces is a novel method of visualizing intermolecular interactions by color-coding, short or long contacts, the color intensity indicating the relative strength of the interactions. The least intermolecular interactions are observed in N…C (3.8%), C…C (2.8%), C…O (0.9%), N…N (1.8%), S…C (2.5%), S…H (5%), S…O (0.8%), S…N (0.5%) and S…S (0.1%). The percentage contributions to the total Hirshfeld surface area is show in the fingerprint plots Fig. 8 (i-xiv). The full 2D interaction plot is shown in Fig. xiv. The electrostatic potential is mapped on Hirshfeld Surface using wave function STO-3 G basis set at Hartree-Fock theory over the range of ±30 auFig. 9 [16]. color scale in between −0.21 au (blue) to 1.2 au (red). In the 2D fingerprint plot, *di* is the closest internal distance from a given point on the Hirshfeld surface and *de* is the closest external contacts. The outline of the full fingerprint is shown in gray. The different orientations (ball and stick model) and the corresponding Hirshfeld surfaces are shown. Fig. 9. represents the Electrostatic potential mapped on Hirshfeld surface (different ori-

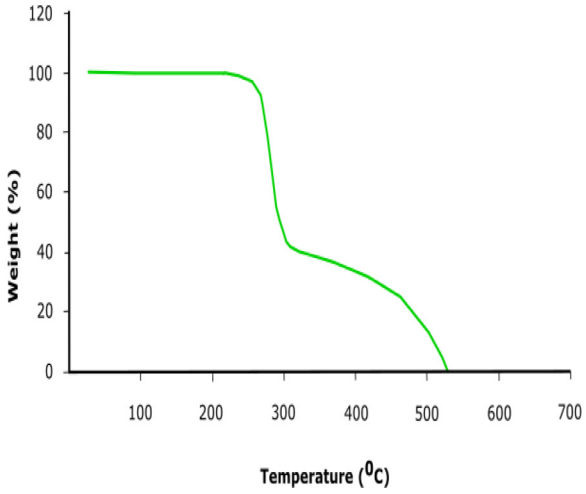

Fig. 4. TGA curve.

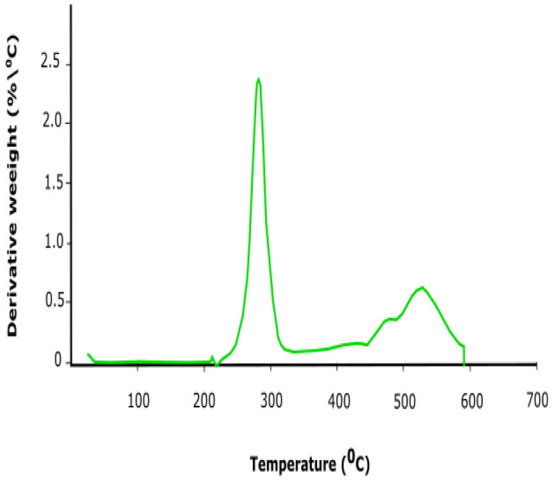

Fig. 5. DTA curve.

entations) with ±30 au Red regions correspond to negative electrostatic potential and blue region corresponds to positive electrostatic potential. The blue region (positive electrostatic potential) over the surface represents the hydrogen donor potential, whereas the hydrogen bond acceptors are represented by red region (negative electrostatic potential). Table 3 gives the percentage contribution of various intermolecular contacts to the Hirshfeld surface.

4. Biological activities

4.1. Mosquito larvicidal activity

The synthesized crystal was screened for the mosquito larvicidal activity in accordance with the WHO guidelines (World Health Organization, 2005) [17]. Three mosquito larvae, viz., *Aedes aegypti, Culex quinquefasciatus* and *Anopheles stephensi* were used for screening. The experiment was performed using late third instar mosquito larvae in sterile 250 mL glass beaker. The 50 mg of crystals were ground into a fine powder and dissolved in 50 mL distilled water along with negative control containing 1 mL acetone with 0.001% Tween-80, kept with each set of the experiment. Temephos, an organophosphate larvicide used to control disease-carrying insects including mosquitoes, was used as the positive control. Ten mosquito larvae from three different species were added to the test sample and the control. The mortality rate of the larvae was recorded after 24 h of incubation at room temperature. The experiment was carried out in triplicates for each of the target compound and their mean (±SD) values were taken. The Median lethal concentration (LC_{50}) with ±95% confidence limit was calculated using Abbott's formula (1925) and Log probit analysis, and results are expressed as ppm. Experimental results are presented in the Table 4.

The larvicidal activity in terms of LC_{50} is inversely proportional to toxicity. A compound with a lower LC_{50} is more toxic than one which has a higher LC_{50}.

Hence, among the three test species the compound (5) was more sensitive towards *A. aegypti* and also exhibits good sensitivity towards other two species *C. quinquefasciatus* and *A. stephensi.* The larvicidal activity of this compound was equivalent to the compound that we reported in our previous paper [8]

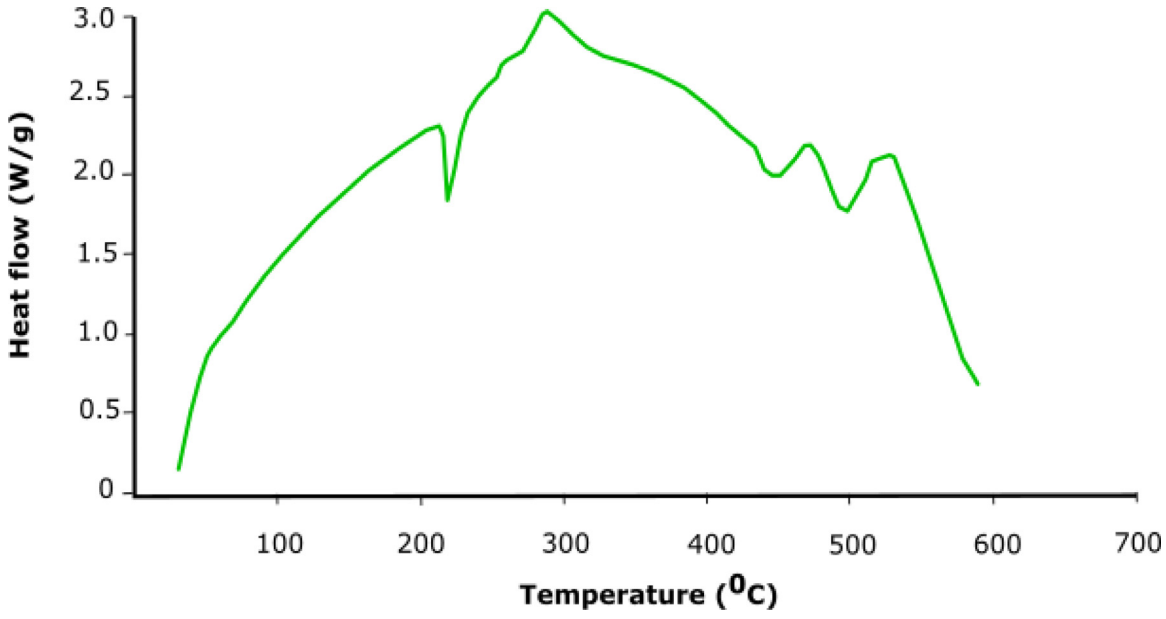

Fig. 6. DSC curve.

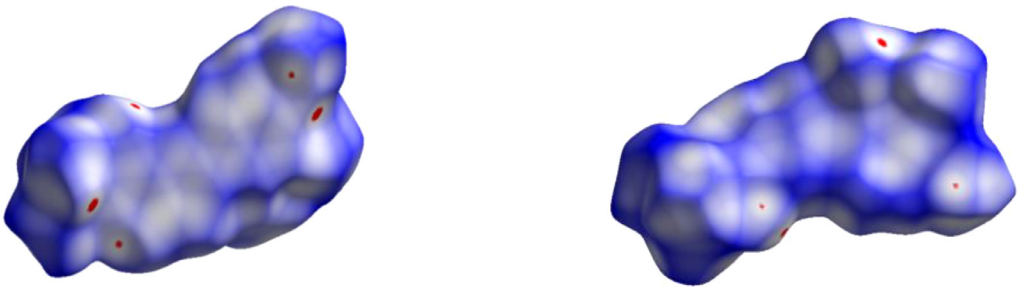

Fig. 7. Hirshfeld surfaces and their corresponding 2D finger print plots of molecule (5).

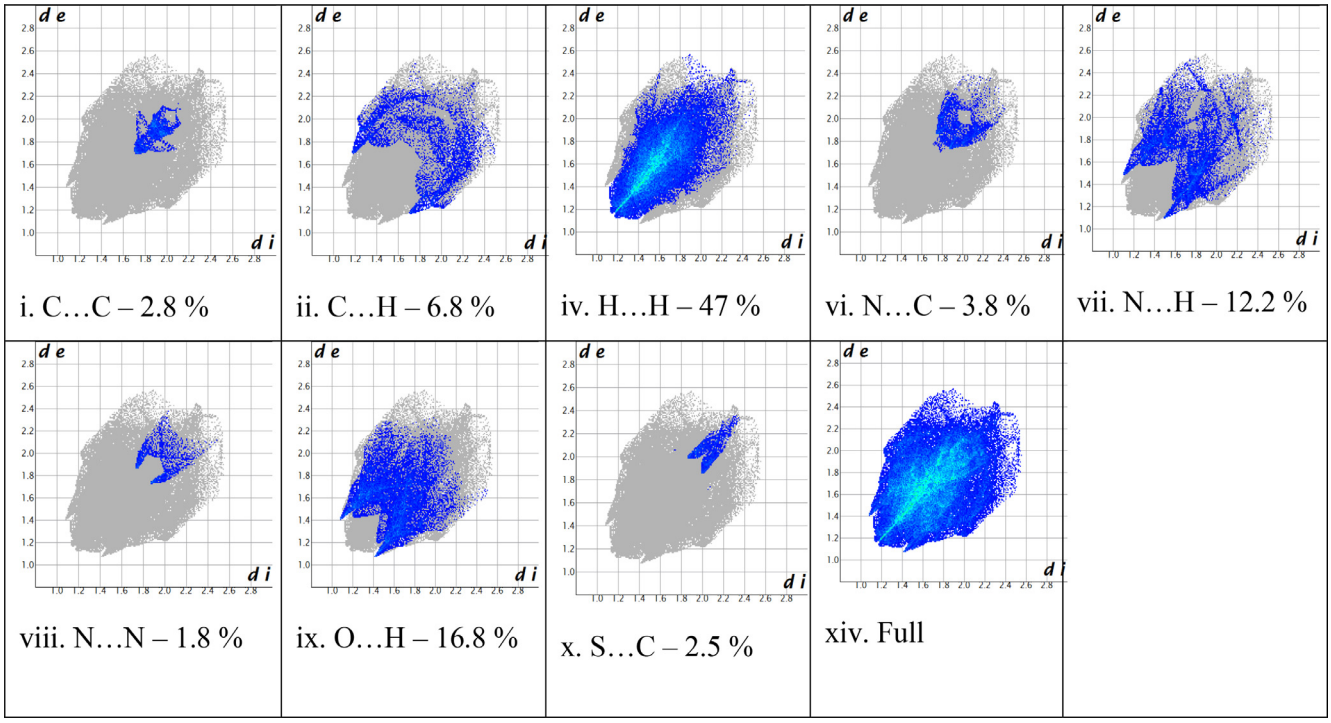

Fig. 8. dnorm mapped on Hirshfeld surface for visualizing the intercontacts of the compound (5) (i-xiv).

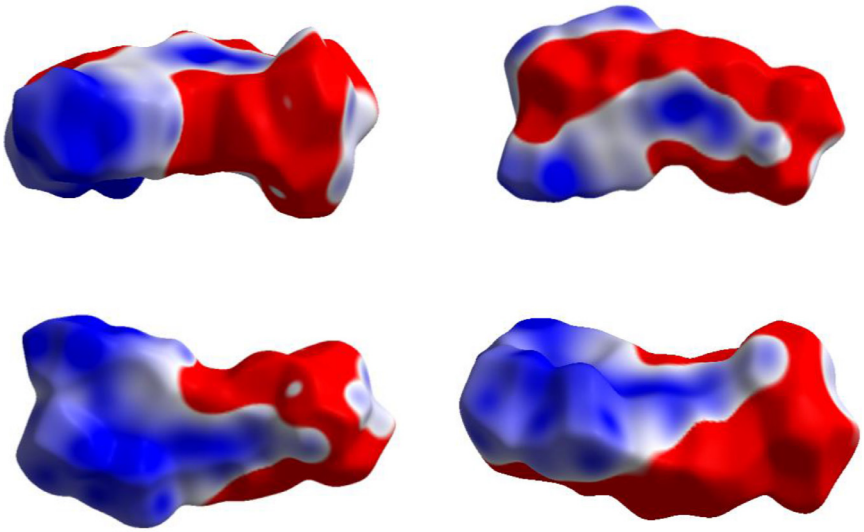

Fig. 9. Electrostatic potential mapped on Hirshfeld surface (different orientations) with ±30 au Red regions correspond to negative electrostatic potential and blue region corresponds to positive electrostatic potential.

Table 3
Percentage of various intermolecular contacts contributing to Hirshfeld surface in triazinone crystal.

Intercontacts	Percentage contribution(%)	Intercontacts	Percentage contribution(%)
H…H	47.0	S…C	2.5
H…O	16.8	N…N	1.8
N…H	12.2	C…O	0.9
C…H	6.8	S…O	0.8
S…H	5	S…N	0.5
N…C	3.8	S…S	0.1
C…C			

Table 4
Mosquito larvicidal activity.

Test Compound (ppm)	A. aegypti		C. quinquefasciatus		A. stephensi	
	LC-50(±95% CI)	LC-90(±95% CI)	LC-50(±95% CI)	LC-90(±95% CI)	LC-50(±95% CI)	LC-90(±95% CI)
Control	–	–	–	–	–	–
[5]	0.625(0.475 – 0.787)	1.9375(1.493- 2.425)	0.7143(0.525 – 0.880)	2.1423(1.602 – 2.696)	0.8334(0.629- 1.054)	3.667(2.640 – 4.624)
Temephos	0.019 (0.013 – 0.024)	0.0612(0.045- 0.076)	0.016(0.012 – 0.019)	0.049(0.036 - 0.063)	0.017(0.013 –0.021)	0.078(0.056 – 0.100)

CI = Confidence limit.
LC50 +.

Table 5
Antifungal activity.

Zone of inhibition(mm±SD)				
Compound(mg/mL)	*C. albicans*	Cladosporium sp.	*A. niger*	T. viride
[5]	20.09 ± 0.45	–	15.16 ± 0.28	10.32 ± 0.25
Fluconazole	26.3 ± 0.30	22.46 ± 0.37	20.73 ± 0.64	23.6 ± 0.52

The LC_{50} is inversely proportional to toxicity. A substance with a lower LC_{50} is more toxic than one which has a higher LC_{50}.

4.2. Antifungal activity

The antifungal activity of the compound (5) was tested by potato dextrose agar well diffusion method [17–22], the microorganisms used for the screening studies are mycelial fungi *Aspergillus niger* ATCC 16,404, Cladosporium sp. ATCC 16,022, the yeast Candida albicans ATCC 10,231 and Trichoderma viride ATCC 28,020. Suspension of fungal strains 100 μL prepared in physiological saline (0.85% NaCl) was spread on Sabouraud dextrose agar (SDA). Sterilized filter paper discs (6.5 mm in diameter) were impregnated with 50 μL of the samples dissolved in dimethyl sulfoxide (DMSO; 1 mg/mL), and placed on the inoculated agar plates. Negative control was prepared using DMSO. Fluconazole was used as the positive control. The inoculated plates were kept at room temperature for 10 min and incubated at room temperature (48 h). The antifungal activity was evaluated by measuring the zone of inhibition against the test fungal pathogens. Experiments were performed in triplicates and standard deviation was calculated. The results are summarized in Table 5. The antifungal screening studies of the compound (5) showed its greater sensitivity towards *C. albicuns,* moderate activity towards *A. niger* and T. viride, but it was totally inactive against Cladosporium *sp*.

5. Conclusions

Single crystal of 3–*tert*–butyl–7-(2,3,4-trimethoxyphenyl)–4*H*-[1,3,4]thiadiazolo[2,3-*c*][1,2,4]triazin-4-one was grown by slow evaporation method at room temperature. The X-Ray diffraction technique was used to confirm the single crystal and to find the lattice parameters. Spectroscopic methods were used to identify the functional group and to determine the chemical environment of grown crystal. The UV–Vis–NIR spectrum showed that the crystal has a broad transparency between 218 nm and 800 nm. The thermal studies were investigated by TG/DTA experiment, which indicated the thermal stability of crystal up to 260.65 °C. The biological screening studies revealed that the grown crystal possesses potential larvicidal and antifungal activities that can be further explored. The observed activities may due to the properties of moieties such as carbonyl and methoxy groups.

Authorship statement

Category1: Conception and design of Study

1 Jagadeesh Prasad Dasappa
2 B. Shivarama Holla
3 Gayathri B. H

Acquisition Data

1 Chandraprabha V. J
2 Ravindra R. Kamble
3 Jagadeesh Prasad Dasappa

Analysis and / or interpretation of data

1 Jagadeesh Prasad Dasappa
2 Prashantha Naik
3 Madan Kumar S

Category2: Drafting of the Manuscript

- Chandraprabha V. J
- Jagadeesh Prasad Dasappa
- Prashantha Naik
- Gayathri B. H

Revising the manuscript critically for important intellectual content

1 Jagadeesh Prasad Dasappa
2 B. Shivarama Holla
3 Prashantha Naik

4 Ravindra R. Kamble
5 Madan Kumar S

Category3:Apporval of the version of the manuscript to be published

1 Chandraprabha V. J
2 Jagadeesh Prasad Dasappa
3 Gayathri B. H
4 Madan Kumar S
5 B. Shivarama Holla
6 R. R. Kamble
7 Prashantha Naik

Declaration of Competing Interest

The authors express that they have no conflict of interest

Acknowledgements

Authors are thankful to the director, SAIF-STIC, Cochin University of science and technology for providing spectroscopic data. The authors thank the DST-PURSE Lab for single crystal X-ray diffractometer, and to Dr. Kishore G. Bhat, Maratha Mandal NGH Institute of Dental Science & Research center, Belgaum, Karnataka, India for providing the fungal strains and lab facilities. Thermogravimateric and UV-visible studies. MKS Thank IOE, Vijnana Bhavana, University of Mysore, Mysore.

References

[1] Sraa Abu-Melha, Synthesis, antimicrobial evaluation and spectroscopic characterization of novel imidazolone, triazole and triazinone derivatives, Spectrochimica Acta Part A: Molecular and Biomolecular Spectroscopy 96 (2012) 898–905, doi:10.1016/j.saa.2012.04.068.
[2] L.S. Pustoshnaya, V.P. Pustoshnyi, A.K. Mazitova, V.K. Khamaev, E. Ya. Davydov, G.E. Zaikov, K.S. Minsker, Antioxidant effect of triazinone derivatives in thermal oxidation of polyisoprene, Polym. Degrad. Stab. 70 (2000) 39–41, doi:10.1016/S0141-3910(00)00079-3.
[3] Tarik El-Sayed Ali, Synthesis and antibacterial activity of some new thiadiaza/triaza phospholes, thiadiaza/triaza/tetrazaphosphinines and thiadiaza/triaza/tetrazaphosphepines containing 1,2,4-triazinone moiety, Eur. J. Med. Chem. 44 (2009) 4539–4546, doi:10.1016/j.ejmech.2009.06.022.
[4] V.J. Chandraprabha, D.Jagadeesh Prasad, Prashantha Naik, Antibacterial and anti tubercular studies of some novel triazinone derivatives, Int. J. Adv. Res. 4 (2016) 1420–1427, doi:10.21474/IJAR01/1942.
[5] K. Sztanke, K. Pasternak, M. Sztanke, M. Kandefer-Szerszeń, A.E. Kozioł, I. Dybała, Crystal structure, antitumour and antimetastatic activities of disubstituted fused 1,2,4-triazinones, Bioorg. Med. Chem. Lett. 19 (2009) 5095–5100, doi:10.1016/j.bmcl.2009.07.036.
[6] N. Vela, J. Fenoll, I. Garrido, G. Navarro, M. Gambín, S. Navarro, Photocatalytic mitigation of triazinone herbicide residues using titanium dioxide in slurry photoreactor, Catal. Today. 252 (2015) 70–77, doi:10.1016/j.cattod.2014.12.011.
[7] G. Schmahl, H. Mehlhorn, Treatment of fish parasites: 6. Effects of sym. triazinone (toltrazuril) on developmental stages of *Glugea anomala*, Moniez, 1887 (microsporidia): A light and electron microscopic study, European Journal of Protistology 24 (1989) 252–259, doi:10.1016/S0932-4739(89)80062-8.
[8] P.A. Castelino, Prashantha Naik, D. Jagadeesh Prasad, R.S. Sujayraj, K. Sharath Chandra, C. Kumara, N. Ramya, M.V. Sandya Kumari, K. Guruprasad, A. Satish Kumar, Synthesis of novel thiadiazolotriazin-4-ones and study of their mosquito- larvicidal and antibacterial properties, Eur. J. Med. Chem. 84 (2014) 194–199, doi:10.1016/j.ejmech.2014.06.072.
[9] Rigaku CrystalClear SM Expert. Rigaku Corporation, (2011) Tokyo, Japan.
[10] (a) G.M. Sheldrick, A short history of *SHELX*, Acta Crystallogr A64 (2008) 112–122 A, doi:10.1107/S0108767307043930; (b) G.M. Sheldrick, Crystal structure refinement with *SHELXL*, Acta Crystallogr C C71 (2015) 3–8, doi:10.1107/S2053229614024218.
[11] C.F. Macrae, I.J. Bruno, J.A. Chisholm, P.R. Edgington, P. McCabe, E. Pidcock, L. Rodriguez-Monge, R. Taylor, J.van de Streek, P.A. Wood, *Mercury CSD 2.0* – new features for the visualization and investigation of crystal structures, J. Appl. Cryst 41 (2008) 466–470, doi:10.1107/S0021889807067908.
[12] S.Madan Kumar S, Fares Hezam Al-Ostoot, B.C. Manjunath, Shamprasad Varija Raghu, E.M. Yasser Hussein, N. Mahesh, A.K. Shaukath, N.K. Lokanath, K. Byrappa, Crystal packing analysis of 1-(3,4-dimethoxyphenyl)-3-(4-bromophenyl)prop-2-en-1-one exhibiting a putative halogen bond C-Br···O, J. Mol. Struct. 1156 (2018) 216–223, doi:10.1016/j.molstruc.2017.11.094.
[13] S.K. Wolff, D.J. Grimwood, J.J. McKinnon, D. Jayatilaka, M.A. Spackamn, Crystal Explorer 3.0, University of Westren Australia, Perth, 2007.
[14] M.A. Spackman, J.J. McKinnon, Fingerprinting intermolecular interactions in molecular crystals, CrystEngComm 66 (2002) 378–392, doi:10.1039/B203191B.
[15] S.M. Kumar, B.C. Manjunath, G.S. Lingaraju, M.M.M. Abdoh, M.P. Sadashiva, N.K. Lokanath, A Hirshfeld Surface Analysis and Crystal Structure of 2'-[1-(2-Fluoro-Phenyl)-1H-tetrazol-5-Yl]-4-Methoxy-Biphenyl-2-Carbaldehyde, Crystal Structure Theory and Applications 2 (2013) 124–131 https://doi:, doi:10.4236/csta.2013.23017.
[16] M.A. Spackmann, J.J. McKinnon, D. Jayatilaka, Electrostatic potentials mapped on Hirshfeld surfaces provide direct insight into intermolecular interactions in crystals CrystEngComm 10 (2008) 377–388, doi:10.1039/B715227B.
[17] Word Health Organization (WHO)Instructions for determining the susceptibility or resistance of mosquito larvae to insecticides, 2005 WHO/CDS/WHOPES/GCDPP/2005.13..
[18] Varaprasad Bobbarala, Prasanth Kumar Katikala, K.Chandrasekhar Naidu, Somasekhar Penumajji, Antifungal activity of selected plant extracts against phytopathogenic fungi Aspergillus niger F2723, Indian J. Sci & Technol. 2 (2009) 4, doi:10.17485/ijst/2009/v2i4/29438.
[19] Rachana Joshi, Nidhi Pandey, KumarYadav Swatantra, Ragini Tilak, Hirdyesh Mishra, Sandeep Pokharia, Synthesis, spectroscopic characterization, DFT studies and antifungal activity of (E)-4-amino-5-[N'-(2-nitro-benzylidene)-hydrazino]-2,4-dihydro-[1,2,4] triazole-3-thione, J. Mol. Struct. 1164 (15) (2018) 386–403, doi:10.1016/j.molstruc.2018.03.081.
[20] Sandeep Chandrashekharappa, Katharigatta N. Venugopala, Susanta K. Nayak, Raquel M. Gleiser, Daniel A. García, Hezekiel M. Kumalo, Rashmi S. Kulkarni, Fawzi M. Mahomoodally, Rashmi Venugopala, Mahendra K. Mohan, Bharti Odhav, One-pot microwave assisted synthesis and structural elucidation of novel ethyl 3-substituted-7- methylindolizine-1-carboxylates with larvicidal activity against *Anopheles arabiensis*, J. Mol. Struct. 1156 (15) (2018) 377–384, doi:10.1016/j.molstruc.2017.11.131.
[21] Ranjan K. Mohapatra, Ashish K. Sarangi, Mohammad Azam, Marei M.El-ajaily MdKudrat-E- Zahan, Suyanbhu B. Patjoshi, Dhruba C. Dash, J. Mol. Struct. 1179 (5) (2019) 65–75, doi:10.1016/j.molstruc.2018.10.070.
[22] YahyaNural MugeGemili, BurcuAydıner ErginKeleş, MahmutÜlger ErtanŞahin NurgülSeferoğlu, ZeynelSeferoğlu SelmaErat, Novel highly functionalized 1,4-naphtho quinone 2-iminothiazole hybrids: Synthesis, photophysical properties, crystal structure, DFT studies, and anti(myco)bacterial/antifungal activity, J. Mol. Struct. 1196 (15) (2019) 536–546, doi:10.1016/j.molstruc.2019.06.087.